Kondo Metal and Ferrimagnetic Insulator on the Triangular Kagome Lattice

Yao-Hua Chen,[1] Hong-Shuai Tao,[1] Dao-Xin Yao,[2,*] and Wu-Ming Liu[1,†]

[1]*Beijing National Laboratory for Condensed Matter Physics, Institute of Physics, Chinese Academy of Sciences, Beijing 100190, China*

[2]*State Key Laboratory of Optoelectronic Materials and Technologies, Sun Yat-sen University, Guangzhou 510275, China*

(Received 16 January 2012; published 13 June 2012)

We obtain the rich phase diagrams in the Hubbard model on the triangular kagome lattice as a function of interaction, temperature, and asymmetry by combining the cellular dynamical mean-field theory with the continuous time quantum Monte Carlo method. The phase diagrams show the asymmetry separates the critical points in the Mott transition of two sublattices on the triangular kagome lattice and produces two novel phases called plaquette insulator with a clearly visible gap and a gapless Kondo metal. When the Coulomb interaction is stronger than the critical value U_c, a short range paramagnetic insulating state, which is a candidate for the short rang resonating valence-bond spin liquid, emerges before the ferrimagnetic order is formed independent of asymmetry. Furthermore, we discuss how to measure these phases in future experiments.

DOI: 10.1103/PhysRevLett.108.246402 PACS numbers: 71.30.+h, 05.30.Rt, 71.10.Fd, 75.10.−b

Geometrically frustrated systems have shown a lot of interesting phenomena such as the spin liquid and spin ice [1–12]. The charge and magnetic order driven by interaction is still one of the central issues in the field of strongly correlated systems [13–21]. Recently, a new class of two-dimensional materials $Cu_9X_2(cpa)_6 \cdot xH_2O$ (cpa=2-carboxypentonic acid, a derivative of ascorbic acid; $X = F$, Cl, Br) has been found [22–24], which is formed by an extra set of triangles (B sites in Fig. 1) inside of the kagome triangles (A sites in Fig. 1). The Cu spins form a new type of geometrically frustrated lattice called triangular kagome lattice (TKL). This lattice can also be realized by cold atoms in the optical lattices, in which the interaction between trapped atoms can be tuned by Feshbach resonance [25–31]. Although the effective spin models on this system have been investigated [32–34], the real charge dynamics with spins and the phase diagram on this lattice have not been studied. In contrast to other frustrated systems such as the triangular lattice and kagome lattice, the "triangles-in-triangles" structure on the TKL induces two different sublattices. Therefore, it is desirable to investigate the Mott and magnetic transition on the TKL under the influence of asymmetry which is induced by different hoppings between two sublattices.

Recently, many analytical and numerical methods have been developed to investigate the strongly correlated system [35–42], such as the dynamical mean-field theory (DMFT) [43]. However, the DMFT works ineffectively in the frustrated systems because the nonlocal correlation and spatial fluctuations are ignored. Therefore, a new method called cellular dynamical mean-field theory (CDMFT) has been developed to incorporate spatially extended correlations and geometrical frustration into the framework of DMFT [44–47] by mapping the original lattice problem onto an effective cluster model coupled to an effective medium. The continuous time quantum Monte Carlo method (CTQMC) [48] is employed as an impurity solver in the CDMFT loop, which is more accurate than the traditional QMC method due to the absence of Trotter decomposition. Therefore, the CDMFT combined with the CTQMC method can provide useful numerous insights into the phase transitions in the frustrated system [17,45].

In the present Letter, we employ the CDMFT combined with the CTQMC method to investigate the influence of

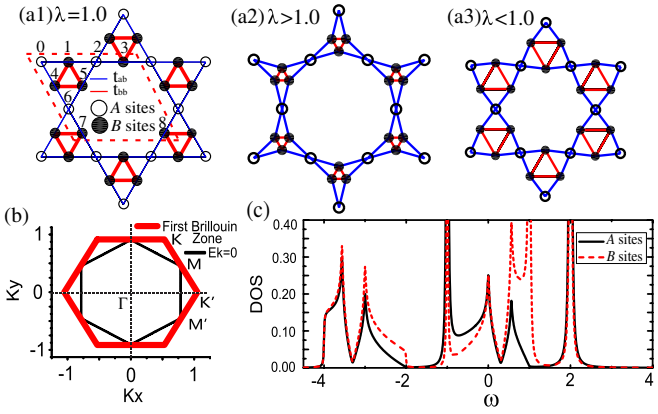

FIG. 1 (color online). (a1) The unit cell of the symmetric TKL ($\lambda = 1$). The open circles denote A sites and the solid circles denote B sites. The blue lines (thin solid lines) represent the hopping between A sites and B sites. And the red lines (thick solid lines) denote the hopping between B sites. (a2) When $\lambda > 1$, the TKL is similar to the kagome lattice. (a3) When $\lambda < 1$, the TKL is transformed into a system composed of many triangular plaquettes. (b) The thick red lines show the first Brillouin zone of the TKL. The thin black lines correspond to the Fermi surface for the noninteracting case. The Γ, K, M, K', M' points denote the points in first Brillouin zone with different symmetry. (c) The density of states of the symmetric TKL for the A and B sites when $U = 0$ at half filling.

asymmetry on the Mott and magnetic phase transition on the TKL, which is detailed in the Supplemental Material [49]. Two novel phases called plaquette insulator and Kondo metal induced by asymmetry are found in the phase diagram, and their properties are studied by determining the momentum resolved spectra. By defining a magnetic order parameter, we can characterize a ferrimagnetic order for the large interaction on the TKL. The phase diagram with the competition between interaction and asymmetry is provided. In addition, the spectral functions on the Fermi surface for the different interactions and asymmetries are presented. These interesting phases can be probed by angle-resolved photoemission spectroscopy (ARPES) [50], neutron scattering, nuclear magnetic resonance [12], and other experiments.

We consider the standard Hubbard model on the TKL at half filling, $H = -\sum_{\langle ij\rangle\sigma} t_{ij} c^{\dagger}_{i\sigma} c_{j\sigma} + U\sum_i n_{i\uparrow} n_{i\downarrow} + \mu \sum_{i\sigma} n_{i\sigma}$, where t_{ij} is the nearest-neighbor hopping energy, U is the Coulomb interaction, μ is the chemical potential, $c^{\dagger}_{i\sigma}$ and $c_{i\sigma}$ denote the creation and annihilation operators, and $n_{i\sigma} = c^{\dagger}_{i\sigma} c_{i\sigma}$ corresponds to the density operator. The asymmetry factor is defined as $\lambda = t_{ab}/t_{bb}$, which can be adjusted by suppressing samples in experiments. For the convenience, we use $t_{bb} = 1.0$ as the energy unit. As shown in Fig. (1a), there are two sublattices on the TKL called A sites and B sites. The space group of the TKL is $p6m$: the same as the honeycomb lattice when $\lambda = 1$ [see Fig. (1a1)]. Figure (1a2) shows the TKL is similar to the kagome lattice when $\lambda > 1$. When $\lambda < 1$, we find the TKL is transformed into a system composed of many triangular plaquettes [see Fig. (1a3)]. The first Brillouin zone and Fermi surface of the symmetric TKL ($\lambda = 1$) with $U = 0$ is shown in Fig. (1b). The density of states (DOS) for different sublattices is similar around the Fermi surface when $U = 0$ and $\lambda = 1$ [see Fig. (1c)].

The phase diagram obtained at $\lambda = 0.6$ shows two coexisting phases when half filled. The asymmetry causes the separation of the phase transition points of the A and B sites. As shown in Fig. 2, with an increasing interaction at $T = 0.5$, the A sites are found to translate from a metallic phase into an insulating phase, and the B sites stay in the insulating phase. This phase is called plaquette insulator (see Fig. 2). In this plaquette insulator, electrons are localized on the A sites, and the absence of next nearest-neighbor hoppings causes the electrons to only be itinerant within the B sites. When $T < 0.34$, the B sites translate into the insulating phase; however, the A sites remain in the metallic phase (see Fig. 2). This coexisting phase corresponds to a Kondo metal. The localized electrons on the B sites act as the magnetic impurity, and the electrons on the A sites are still highly itinerant. In this phase, the system shows the strong Kondo effect because of the high density of magnetic impurities. When $U > U_c$, i.e., $U_c = 7.8$ at $T = 0.25$, both the A and B sites transform into insulators. In Fig. 2, we find a reentrant behavior in the Mott transition

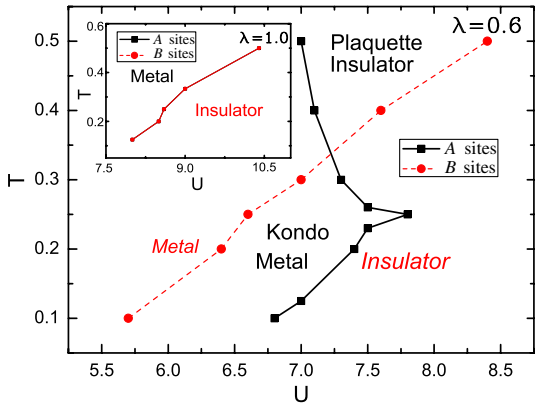

FIG. 2 (color online). Phase diagram of the TKL at $\lambda = 0.6$. The black solid lines show the transition line of the A sites, and the red dashed lines show the transition line of the B sites. Two kinds of coexisting phases between red lines and black lines are the plaquette insulator and Kondo metal. Inset: The phase diagram of the symmetric TKL ($\lambda = 1$), in which there are no coexisting phases.

of the A sites caused by the frustration and asymmetry, which is also found in the anisotropic triangular lattice [19]. This reentrant behavior divides the coexisting phases into two parts: the plaquette insulator and Kondo metal. The inset figure in Fig. 2 shows the phase diagram of the TKL at $\lambda = 1$. There are no coexisting phases and reentrant behaviors found when the asymmetry is absent.

In order to find the properties of the different phases in Fig. 2, we investigate the momentum resolved spectrum $A_k(\omega)$ by using the maximum entropy method [51]. The

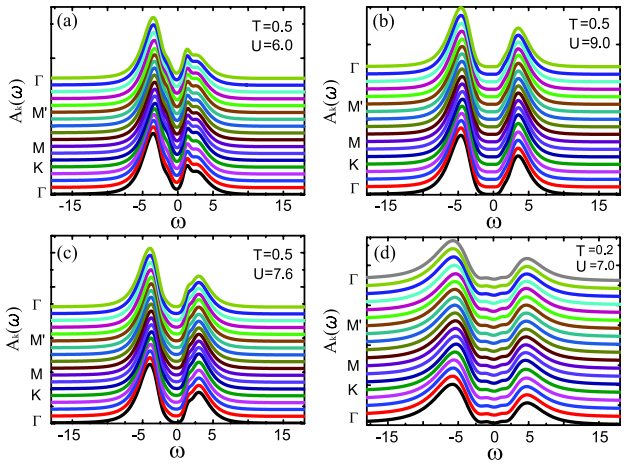

FIG. 3 (color online). The momentum resolved spectrum $A_k(\omega)$ at $\lambda = 0.6$. (a) The metallic phase at $U = 6$ and $T = 0.5$. (b) The Mott insulating phase at $U = 9$ and $T = 0.5$. A clearly visible single particle gap shows up around the Fermi energy. (c) The plaquette insulating phase at $U = 7.6$ and $T = 0.5$, in which A sites are insulating, but B sites are metallic. A small gap shows up in this phase. (d) The Kondo metallic phase at $U = 7$ and $T = 0.2$, in which A sites are metallic and B sites are insulating. The single particle gap vanishes in this phase.

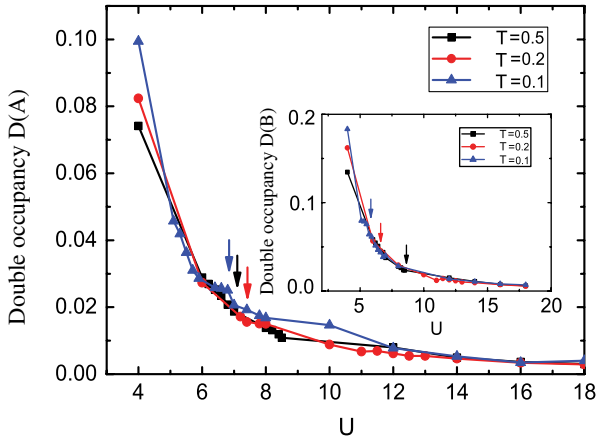

FIG. 4 (color online). The evolution of double occupancy D on the A sites as a function of U with different temperatures at $\lambda = 0.6$. The inset figure shows the evolution of double occupancy on the B sites. The arrows with different colors show the phase transition points at different temperatures.

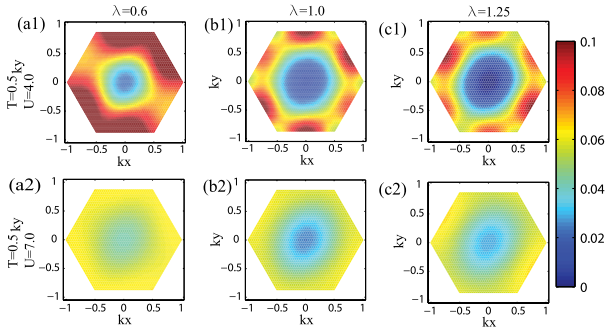

FIG. 5 (color online). The evolution of the spectral function on Fermi surface. (a) $\lambda = 0.6$. (b) $\lambda = 1$. (c) $\lambda = 1.25$.

results are shown in Fig. 3. The Γ, K, M and M' points have been defined in Fig. (1b). When $T = 0.5$ and $U = 6$, we find two obvious quasiparticles near $\omega = -4$ and $\omega = 2$ [see Fig. 3(a)]. The gapless behavior shows that the system stays in the metallic phase shown in Fig. 2. When U increases, we find a clearly visible gap near the Fermi energy [see Fig. 3(b)], which indicates the system becomes an insulator, denoted in Fig. 2. $A_k(\omega)$ of the plaquette insulator is shown in Fig. 3(c). In Fig. 3(d), we find there is no clearly visible gap near the Fermi energy when the system stays at the Kondo metal state in Fig. 2. The momentum resolved spectral function can be obtained by the ARPES experiment, and the plaquette insulator and Kondo metal can be found in real samples. We define the double occupancy D on the TKL as $D = \partial F/\partial U = \frac{1}{N}\sum_i \langle n_{i\uparrow} n_{i\downarrow}\rangle$, where F is the free energy and N denotes the number of lattice sites. In Fig. 4, the decreasing of D on both sublattices shows the suppressing of the itinerancy of electrons, which is a characteristic behavior of the Mott transition. When the temperature drops, D increases due to the enhancement of spin fluctuation at low temperature. The arrows indicate the phase transition point at different temperatures. The smoothly decreasing D characterizes a second order Mott transition when the interaction U increases.

In Fig. 5, we show the evolution of spectral function on a Fermi surface as a function of $\mathbf{k}$ for different U, T, and λ, which is defined as $A(\mathbf{k}; \omega = 0) \approx -\lim_{\omega\to 0} \mathrm{Im} G_{\mathbf{k}}(\omega + i0)/\pi$, where $G_{\mathbf{k}}(\omega)$ is the $\mathbf{k}$-dependent Green's function and $\mathbf{k}$ is the wave vector in the original Brillouin zone. When $\lambda = 1$ [see Fig. (5b1)], the spectral function shows six peaks near the M point in Fig. (1b), similar to the noninteracting case. When U increases, the Fermi surface shrinks because of the localization of electrons. Figure (5a1) shows the Fermi surface is similar to the system composed of many triangular plaquettes at $\lambda = 0.6$. The Fermi surface at $\lambda = 1.25$ is similar to a kagome lattice [see Fig. (5c1)]. When U keeps increasing, the Fermi surface is developing into a flat plane showing the localization of electrons [see Figs. (5a2)–(5c2)]. The spectral function can be measured by ARPES experiments.

In order to investigate the evolution of magnetic order on the TKL, we define a ferrimagnetic order parameter by $m = \frac{1}{N}\sum_i \mathrm{sgn}(i)(\langle n_{i\uparrow}\rangle - \langle n_{i\downarrow}\rangle)$, where i denotes the lattice index shown in Fig. (1a1), and N is the number of lattice sites. We define $\mathrm{sgn}(i) = 1$, for $i = 0, 2, 6$; and $\mathrm{sgn}(i) = -1$, for $i = 1, 3, 4, 5, 7, 8$. Figure 6 shows the evolution of a single particle gap ΔE and m as a function of U when $\lambda = 1$ and $T = 0.2$. The Mott transition points of the A and B sites coexist when the asymmetry is absent. A gap opens when $U = 8.5$. The ferrimagnetic order parameter $m = 0$ at $U < U_c = 13.8$ indicates the system is in a paramagnetic insulating state. This nonmagnetic state, in which

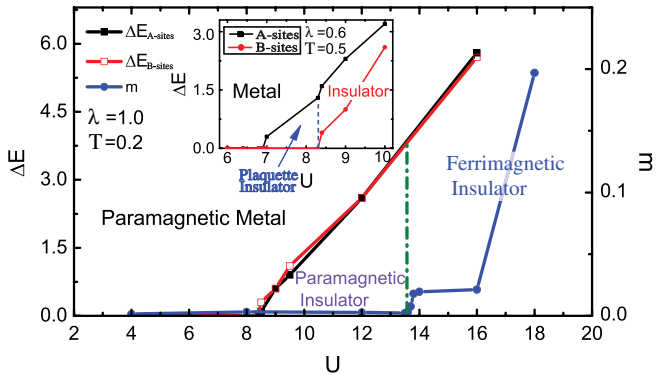

FIG. 6 (color online). The evolution of single particle gap ΔE and ferrimagnetic order parameter m at $\lambda = 1$ and $T = 0.2$. A paramagnetic metallic phase is found when U is weak with $\Delta E = 0$ and $m = 0$. As U increases, a gap is opened and no magnetic order is formed with $\Delta E \neq 0$ and $m = 0$. This paramagnetic insulating state can be a short range RVB spin liquid. An obvious magnetic order is formed when U is strong enough with $\Delta E \neq 0$ and $m \neq 0$. The inset picture shows the evolution of ΔE at $\lambda = 0.6$ and $T = 0.5$. A plaquette insulator is found when the A sites are insulating, and the B sites are metallic.

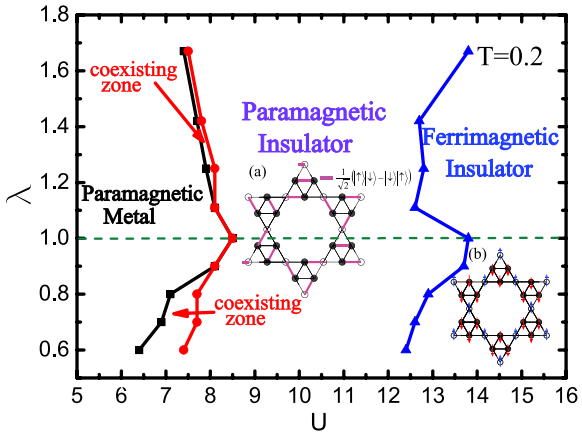

FIG. 7 (color online). The phase diagram of the TKL represents the competition between U and λ for $T = 0.2$. The region between the black lines and the red lines denotes the coexisting zone which contains the plaquette insulator and the Kondo metal parts. A wide paramagnetic insulating region is found with an intermediate U. The blue lines show the transition point to the ferrimagnetic insulator with a clear magnetic order. Inset: (a) One possible dimer configuration formed in the paramagnetic insulator, which is a candidate for the short range RVB spin liquid. (b) Spin configuration of ferrimagnetic insulator.

there is a visible gap, is similar to the short range resonating-valence-bond state (RVB) found in other systems, such as the honeycomb lattice [3,6,16]. We argue that this paramagnetic insulating state is a candidate for the short range RVB spin liquid due to the absence of any long range correlations. There is a large region in the parameter space where the RVB spin liquid state is favored. When $U > U_c$, the finite m means the system enters a ferrimagnetic state. The inset picture of Fig. 6 shows the evolution of single particle gap ΔE at $\lambda = 0.6$ and $T = 0.5$, in which a gap opens on the A sites first.

Finally, we provide a phase diagram about λ and U at $T = 0.2$ (see Fig. 7). As λ increases, a coexisting zone containing the plaquette insulator and the Kondo metal shows up. This zone is suppressed from $\lambda = 0.9$ to $\lambda = 1.11$. When $U > U_c$, such as $U_c = 13.8$ at $\lambda = 1$, the system becomes a ferrimagnetic insulator with $m \neq 0$. Before entering the ferrimagnetic phase, a paramagnetic insulator state is found. We argue this paramagnetic insulator state is a candidate for a short range RVB spin liquid due to the absence of any magnetic order and long range correlations.

In summary, we have obtained the rich phase diagrams as a function of interaction U, temperature T, and asymmetry factor λ. The asymmetry introduced in this strongly frustrated system can change the shape of the metal-insulator translation line and induce several interesting phases, such as the plaquette insulator and Kondo metal. In the plaquette insulator phase, a clearly visible gap is found near the Fermi energy by investigating the momentum resolved spectral function. The Kondo metal phase is an interesting phase where the partial sites work as the magnetic impurities in the metallic environment. We also find an interesting paramagnetic insulating state which is related to the short range RVB spin liquid state before the ferrimagnetic order is formed. Also, the increasing of asymmetry does not suppress the emergence of this ferrimagnetic order. In addition, we have presented all kinds of spectra which can be used to detect these phases in real materials, such as $Cu_9X_2(cpa)_6 \cdot xH_2O$, under applied pressure in experiments. Our studies provide a helpful step for understanding the coexisting behavior in metal-insulator transition, the formation of magnetic order, and the emerging of spin liquids in frustrated systems with asymmetry.

We would like to thank N. H. Tong and S. Q. Shen for valuable discussions. This work was supported by the NKBRSFC under Grants No. 2011CB921502, No. 2012CB821305, No. 2012CB821400, No. 2009CB930701, and No. 2010CB922904 and NSFC under Grants No. 10934010, No. 60978019, and No. 11074310 and NSFC-RGC under Grants No. 11061160490 and No. 1386-N-HKU748/10, NCET-11-0547, and RFDPHE of China (20110171110026).

*yaodaox@mail.sysu.edu.cn
†wmliu@iphy.ac.cn

[1] S. T. Bramwell *et al.*, Nature (London) **461**, 956 (2009).
[2] E. Mengotti, L. J. Heyderman, A. F. Rodríguez, F. Nolting, R. V. Hügli, and Hans-Benjamin Braun, Nature Phys. **7**, 68 (2010).
[3] R. Moessner, S. L. Sondhi, and E. Fradkin, Phys. Rev. B **65**, 024504 (2001).
[4] M. Hermele, T. Senthil, M. P. A. Fisher, P. A. Lee, N. Nagaosa, and X.-G. Wen, Phys. Rev. B **70**, 214437 (2004).
[5] P. A. Lee, N. Nagaosa, and X. G. Wen, Rev. Mod. Phys. **78**, 17 (2006).
[6] L. Balents, Nature (London) **464**, 199 (2010).
[7] S. H. Lee, H. Kikuchi, Y. Qiu, B. Lake, Q. Huang, K. Habicht, and K. Kiefer, Nature Mater. **6**, 853 (2007).
[8] M. A. de Vries *et al.*, Phys. Rev. Lett. **103**, 237201 (2009).
[9] Y. Kurosaki, Y. Shimizu, K. Miyagawa, K. Kanoda, and G. Saito, Phys. Rev. Lett. **95**, 177001 (2005).
[10] Y. Okamoto, M. Nohara, H. Aruga-Katori, and H. Takagi, Phys. Rev. Lett. **99**, 137207 (2007).
[11] B. K. Clark, D. A. Abanin, and S. L. Sondhi, Phys. Rev. Lett. **107**, 087204 (2011).
[12] L. Limot, P. Mendels, G. Collin, C. Mondelli, B. Ouladdiaf, H. Mutka, N. Blanchard, and M. Mekata, Phys. Rev. B **65**, 144447 (2002).
[13] M. Wang *et al.*, Phys. Rev. B **84**, 094504 (2011).
[14] F. Mezzacapo and M. Boninsegni, Phys. Rev. B **85**, 060402 (2012).
[15] P. W. Anderson, Science **235**, 1196 (1987).
[16] Z. Y. Meng, T. C. Lang, S. Wessel, F. F. Assaad, and A. Muramatsu, Nature (London) **464**, 847 (2010).
[17] T. Yoshioka, A. Koga, and N. Kawakami, Phys. Rev. Lett. **103**, 036401 (2009).

[18] Y. Kato, Q. Zhou, N. Kawashima, and N. Trivedi, Nature Phys. **4**, 617 (2008).
[19] T. Ohashi, N. Kawakami, and H. Tsunetsugu, Phys. Rev. Lett. **97**, 066401 (2006).
[20] M. Jarrell and H. R. Krishnamurthy, Phys. Rev. B **63**, 125102 (2001).
[21] W. Wu, Y. H. Chen, H. S. Tao, N. H. Tong, and W. M. Liu, Phys. Rev. B **82**, 245102 (2010).
[22] M. Gonzalez, F. Cervantes-Lee, and L. W. ter Haar, Mol. Cryst. Liq. Cryst. Sci. Technol., Sect. A **233**, 317 (1993).
[23] S. Maruti and L. W. ter Haar, J. Appl. Phys. **75**, 5949 (1994).
[24] M. Mekata, T. Nishino, K. Morishita, H. Tanaka, and K. Iio, J. Magn. Magn. Mater. **177–181**, 731 (1998).
[25] D. Jaksch, C. Bruder, J. I. Cirac, C. W. Gardiner, and P. Zoller, Phys. Rev. Lett. **81**, 3108 (1998).
[26] W. Hofstetter, J. I. Cirac, P. Zoller, E. Demler, and M. D. Lukin, Phys. Rev. Lett. **89**, 220407 (2002).
[27] M. Greiner, O. Mandel, T. Esslinger, T. W. Hänsch, and I. Bloch, Nature (London) **415**, 39 (2002).
[28] L. M. Duan, E. Demler, and M. D. Lukin, Phys. Rev. Lett. **91**, 090402 (2003).
[29] P. Soltan-Panahi *et al.*, Nature Phys. **7**, 434 (2011).
[30] N. Gemelke, X. Zhang, C.-L. Hung, and C. Chin, Nature (London) **460**, 995 (2009).
[31] Y. H. Chen, W. Wu, H. S. Tao, and W. M. Liu, Phys. Rev. A **82**, 043625 (2010).
[32] Y. L. Loh, D. X. Yao, and E. W. Carlson, Phys. Rev. B **77**, 134402 (2008).
[33] D. X. Yao, Y. L. Loh, E. W. Carlson, and M. Ma, Phys. Rev. B **78**, 024428 (2008).
[34] A. Yamada, K. Seki, R. Eder, and Y. Ohta, Phys. Rev. B **83**, 195127 (2011).
[35] D. Galanakis, T. D. Stanescu, and P. Phillips, Phys. Rev. B **79**, 115116 (2009).
[36] K. Aryanpour, W. E. Pickett, and R. T. Scalettar, Phys. Rev. B **74**, 085117 (2006).
[37] C. C. Chang and S. W. Zhang, Phys. Rev. Lett. **104**, 116402 (2010).
[38] W. Yao and Q. Niu, Phys. Rev. Lett. **101**, 106401 (2008).
[39] D. Xiao, W. Yao, and Q. Niu, Phys. Rev. Lett. **99**, 236809 (2007).
[40] H. Lee, G. Li, and H. Monien, Phys. Rev. B **78**, 205117 (2008).
[41] H. Terletska, J. Vučičević, D. Tanasković, and V. Dobrosavljević, Phys. Rev. Lett. **107**, 026401 (2011).
[42] F. Zhou, Phys. Rev. Lett. **87**, 080401 (2001).
[43] A. Georges, G. Kotliar, W. Krauth, and M. J. Rozenberg, Rev. Mod. Phys. **68**, 13 (1996).
[44] T. Maier, M. Jarrell, T. Pruschke, and M. H. Hettler, Rev. Mod. Phys. **77**, 1027 (2005).
[45] H. Park, K. Haule, and G. Kotliar, Phys. Rev. Lett. **101**, 186403 (2008).
[46] L. DeLeo, M. Civelli, and G. Kotliar, Phys. Rev. Lett. **101**, 256404 (2008).
[47] O. Parcollet, G. Biroli, and G. Kotliar, Phys. Rev. Lett. **92**, 226402 (2004).
[48] A. N. Rubtsov, V. V. Savkin, and A. I. Lichtenstein, Phys. Rev. B **72**, 035122 (2005).
[49] See Supplemental Material at http://link.aps.org/supplemental/10.1103/PhysRevLett.108.246402 for the details of CDMFT combining with CTQMC, which is employed to investigate the quantum phase transitions on the TKL.
[50] A. Damascelli, Z. Hussain, and Z. X. Shen, Rev. Mod. Phys. **75**, 473 (2003).
[51] M. Jarrell and J. E. Gubernatis, Phys. Rep. **269**, 133 (1996).